Author response to interactive comment of H. Grothe and M. J. Rossi: "Spectroscopic evidence for large aspherical β-NAT particles involved in denitrification in the December 2011 Arctic stratosphere"

Atmos. Chem. Phys. Discuss., doi:10.5194/acp-2016-146, in review, 2016
W. Woiwode et al.

We would like to thank H. Grothe and M. J. Rossi for their interesting comments, remarks and suggestions to improve the manuscript. In the following, we provide the original short comment (italic letters) followed by our responses. Text added or modified in the revised manuscript is colored in red.

The investigation by Woiwode et al. (2016) represents an improved and updated reinterpretation of spectroscopic data on the existence of NAT particles in the Artic lower stratosphere. However, the whole evidence is based on the symmetric nitrate deformation band $v_2=\delta_s(NO_3^-)$, which is in general the weakest band of the overall mid-infrared spectrum of nitric acid hydrates. Also, the differences between the v_2 bands of NAT (α, β) and NAD (α, β) are rather small. These differences may also be caused by different crystal structures or different morphologies and textures of the very same phase. This might be worth to be mentioned in the text. Unless concomitant changes in other parts of the mid IR spectrum are not conclusively observed, minor changes in one of the IR absorptions alone constitute weak evidence for the reasons cited above.

We initially excluded α-NAT due to too warm temperatures, a weaker signature at 820 cm^{-1}, and the fact that this constituent has not yet been confirmed in the stratosphere from FTIR observations so far to our best knowledge. Furthermore, in our opinion the positions of the v_2 bands of NO_3^- in α/β-NAD are significantly different from α/β-NAT in context of high-resolution infrared observations. We agree that a more detailed discussion of the spectral signatures would be helpful. Furthermore, we would like to clarify that the identification of β-NAT is not limited only to the v_2 band of NO_3^-, but also to characteristic spectral patterns in the entire channels 1 (725-990 cm^{-1}) and 2 (1150-1350 cm^{-1}) of MIPAS-STR.

- The signature around 820 cm^{-1} attributed to the v_2 mode of NO_3^- in β-NAT well exceeds the signal-to noise of the measurements. Therefore, the fact alone that this band has a smaller amplitude than other bands of the same substance does not mean that it is not suitable for identification.

- The spectral signature at 820 cm^{-1} is particularly well suited for identification, since it is located in a region of the spectrum weakly populated by gaseous absorbers and where thermal emission is high relative to other regions covered by the MIPAS-STR observations due to the increase of atmospheric thermal emission towards lower wavenumbers. Furthermore, it represents a sharp feature, having a significant amplitude in both the imaginary and real parts of the refractive indices and resulting in characteristic signatures in the absorption and scattering cross-sections of large highly aspherical β-NAT particles (see response to referee #1). The amplitudes of the 820 cm^{-1} signature of β-NAT in the refractive index imaginary and real parts used here are significantly higher than the corresponding signatures in available refractive indices of α-NAT and (α-)NAD.

- The simulations of the MIPAS-STR spectra using the refractive indices of β-NAT reproduce the signature attributed to the v_2-band of β-NAT in both (i) spectral position and (ii) amplitude and therefore provide a strong hint at β-NAT. As discussed by Höpfner et al. (2006a), many studies consistently report a spectral position at ~809 cm^{-1} for the v_2-band of NO_3^- in (α-)NAD, which is significantly different from the position at ~820 cm^{-1} consistently reported in the

literature for both α-NAT and β-NAT. We are not familiar with any study suggesting a signature at 820 cm^{-1} almost identical to β-NAT in both in position and amplitude for a nitric acid hydrate other than β-NAT.

- The identification of β-NAT not only is based on the v_2 band of NO_3^- in the spectral region around 820 cm^{-1}, but also on refractive index patterns in the entire spectral ranges of MIPAS-STR channels 1 and 2. These cover the broad v_3 asymmetric stretch band of NO_3^- around ~1330 cm^{-1} and the v_2 symmetric umbrella mode of H_3O^+ around ~1200 cm^{-1}, which result in broad, weak and unspecific signatures in the simulated spectra. While in the Mie simulations, the channel 2 spectra are almost identical for the considered nitric acid hydrate modifications, notable differences are found in the comparison with STS and ice. Within the simulations of nitric acid hydrates, the combination of the specific signature around 820 cm^{-1} of β-NAT with the unspecific signatures in channel 2 and further non-specified distinct patterns (see notable differences between Mie scenarios of β-NAT, α-NAT (see below) and NAD in channel 1 above 830 cm^{-1}) provides a characteristic fingerprint, which becomes more pronounced for aspheric particles.

We included also α-NAT in the analysis and modified the manuscript as follows (text modified in context of the comments by referee #1 is colored in blue.):

P1/L20-22: We analyse polar stratospheric cloud (PSC) signatures in airborne MIPAS-STR (Michelson Interferometer for Passive Atmospheric Sounding – STRatospheric aircraft) observations in the spectral regions from 725 to 990 cm^{-1} and 1150 to 1350 cm^{-1} under conditions suitable for the existence of nitric acid trihydrate (NAT) above northern Scandinavia on 11 December 2011.

P1/L24: v_2 symmetric deformation mode of NO_3^- in β-NAT

P2/L27: To our best knowledge, α-NAT has not been identified in infrared field observations so far.

P7/L17-18: α-NAT, STS and ice are unlikely candidates due to too high temperatures.

P8/L4: For simulating the signatures of α-NAT, we use the refractive indices for α-NAT aerosols by Richwine et al. (1995), which show a more developed signature around 820 cm^{-1} than the corresponding faint signature in the refractive indices for α-NAT by Toon et al. (1994).

P9/L13: Mie calculations of spherical β-NAT, α-NAT, NAD, STS and ice particles

P9/L14: β-NAT, α-NAT, NAD,

P10/L8-11 (discussion of residuals further refined): For α-NAT (Fig. 10c and 10d), NAD (Fig. 10e and 10f), and STS (Fig. 10g and 10h), similar residuals are found for both size distributions when compared to β-NAT. For these species, more “step-like” residual signatures are found in the spectral region around 820 cm^{-1} for both size distributions when compared to β-NAT.

P10/L1511 (discussion of residuals further refined): a “step-like” dip

P10/L19: we exclude α-NAT, NAD,

P10/L21-27:

- β-NAT exhibits a characteristic spectral signature around 820 cm^{-1} and is the only PSC constituent known to be thermodynamically stable under the conditions of the flight.

- The metastable α-NAT modification also exhibits a characteristic spectral signature around 820 cm^{-1} with a weaker amplitude (Höpfner et al. 2006a). However, α-NAT is expected to irreversibly transform into β-NAT at the temperatures around flight altitude (Tizek et al., 2004; compare Fig. 7). Furthermore, laboratory experiments by Grothe et al. (2006) support approximately spherical geometries of α-NAT particles, while the presented Mie calculations for spherical α-NAT particles result only in coarse agreement with the observations.

P12/L16-27: Figure 13c and 13d show the imaginary parts of the refractive indices of β-NAT, α-NAT, NAD, STS and ice, which determine the absorption and emission characteristics of the particles. In the spectral region around 820 cm^{-1}, which is weakly populated by trace gas signatures, β-NAT provides the strongest signature due to the ν_2 symmetric deformation mode of NO_3^-. Further broad peaks are found in channel 2 around ~1330 cm^{-1} due to the ν_3 asymmetric stretch mode of NO_3^- and around ~1200 cm^{-1} due to the ν_2 symmetric umbrella mode of H_3O^+ (Ortega et al., 2006, and references therein). These signatures however result in weak and broad residual patterns in the Mie scenarios, which are unspecific without further information (see Fig.10). The α-NAT refractive index imaginary part also shows a peak at 820 cm^{-1} due to the ν_2 symmetric deformation mode of NO_3^- of this NAT modification. The amplitude is however only about half of the amplitude of the used β-NAT refractive index, and it is superimposed by a broader signature beginning at ~900 cm^{-1} and peaking at ~780 cm^{-1}. Similarly to α-NAT, NAD also shows a peak at 808 cm^{-1} with a smaller amplitude when compared to β-NAT along with another peak with higher amplitude at 745 cm^{-1} in the region densely populated with trace gas signatures. Furthermore, NAD also shows broad peaks at ~1260 cm^{-1} due to the ν_3 mode NO_3^- and at ~1150 cm^{-1} (coinciding with the channel boundary) due to the ν_2 mode of H_3O^+. For α-NAT, only the increasing slopes of the corresponding signatures towards the boundaries of channel 2 can be identified. STS shows no significant peak-like signatures in both channels. For ice, a broad peak spanning the entire range of channel 1 is found due to librational modes in the ice crystal (Zasetsky et al., 2005).

Figures 13e and 13f show the real parts of the refractive indices of the discussed species, which determine the scattering of radiation from outside into the field-of-view. β-NAT shows the strongest "step-like" signature in the spectral region around 820 cm^{-1}, corresponding with the peak in the refractive index imaginary part. α-NAT and NAD again show weaker corresponding signatures at 820 cm^{-1} and 808 cm^{-1}. For NAD, another sharp step is seen at ~745 cm^{-1} and a broad step around ~1270 cm^{-1}. Ice shows an extended decreasing gradient from the lower boundary of channel 1 to ~930 cm^{-1}. Neither ice, nor STS shows any characteristic sharp signature in both channels.

The refractive indices of β-NAT show the strongest signature at 820 cm^{-1} in both the refractive index imaginary and real part and allow to model the "shoulder-like" signature around 820 cm^{-1} with a realistic spectral position and amplitude. α-NAT and NAD also show similar but significantly weaker signatures at 820 cm^{-1} and 808 cm^{-1}, respectively. Therefore, potential highly aspherical large α-NAT and NAD particles are expected to result in considerably weaker corresponding "shoulder-like" signatures along with further discrepancies from β-NAT as a consequence of different patterns in the refractive index imaginary and real parts.

P16/L12: the ν_2 symmetric deformation mode of NO_3^-

P16/L20: The ν_2 symmetric deformation mode of NO_3^- at 820 cm^{-1} is well suited for identification of β-NAT, since it is located in a spectral region weakly populated by gaseous absorbers and where the thermal emission of the atmosphere is higher than at higher wavenumbers. Furthermore, it represents a sharp feature, having a significant amplitude in both the refractive index imaginary and real part. The identification of large aspherical β-NAT particles is furthermore supported by the reasonable overall agreement of the simulations with the observations in the entire spectral regions analyzed, covering further weak and broad signals due to the ν_3 asymmetric stretch mode of NO_3^- around ~1330 cm^{-1}, the

v_2 symmetric umbrella mode of H_3O^+ at ~1200 cm^{-1} and unspecified patterns. The combination of these signatures results in a specific fingerprint in the absorption and scattering cross-sections of highly aspherical large β-NAT particles. Potential highly aspherical large α-NAT and α-NAD particles are expected to result in considerably weaker "shoulder-like" signatures at ~820 cm^{-1} and ~808 cm^{-1} due to weaker corresponding signatures in the refractive indices along with further discrepancies from β-NAT due to different patterns in the refractive indices at higher wavenumbers.

P18/L16-17: We thank U. M. Biermann, L. J. Richwine, R. F. Niedziela and A. Y. Zasetsky for providing the refractive indices of β-NAT, α-NAT, STS, NAD and ice.

P21/L12: Ortega, I. K., Maté, B., Moreno, M. A., Herrero, V. J., and Escribano, R.: Infrared spectra of nitric acid trihydrate (β-NAT): A comparison of available optical constants and implication for the detection of polar stratospheric clouds (PSCs), Geophys. Res. Lett., 33, L19816, doi:10.1029/2006GL026988, 2006.

P21/L24: Richwine, L. J., Clapp, M. L., Miller, R. E., and Worsnop, D. R.: Complex refractive indices in the infrared of nitric acid trihydrate aerosols, Geophys. Res. Lett., 22, 2625–2628, 1995.

P22/L9: Toon, O. B., Tolbert, M. A., Koehler, B. G., Middlebrook, A. M., and Jordan, J.: Infrared optical constants of H_2O ice, amorphous nitric acid solutions, and nitric acid hydrates, J. Geophys. Res., 99(D12), 25631–25654, doi:10.1029/94JD02388, 1994.

P24/Table 1 (scenarios for spherical α-NAT particles added):

ID	Species	Size distribution	Code / aspect ratio (AR)	Vertical PSC extent [km]	Vertical range of trop. cloud [km] / α [km^{-1}]	Comment
49	α-NAT	B	Mie[a] / 1.0	17-23	0-10 / 0.0223	
50	α-NAT	A	Mie[a] / 1.0	17-23	0-10 / 0.0223	

P35 (new Figures 10c and 10d for spherical α-NAT particles):

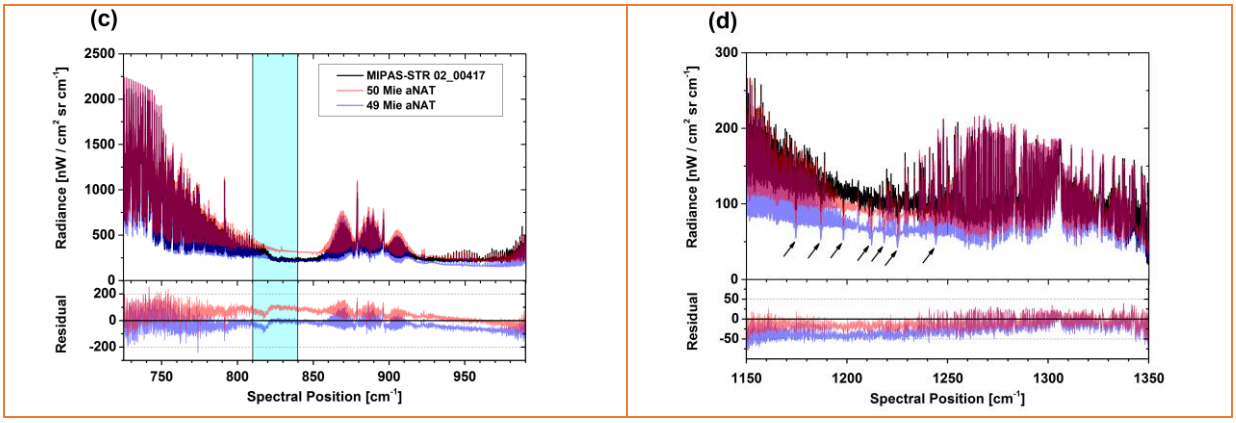

P36/L3-4: Simulations of (a) and (b) β-NAT, (c) and (d) α-NAT, (e) and (f) NAD, (g) and (h) STS, and (i) and (j) ice with size distributions A (red) and B (blue).

P39 (refractive indices of α-NAT included in Figures 13c to 13f):

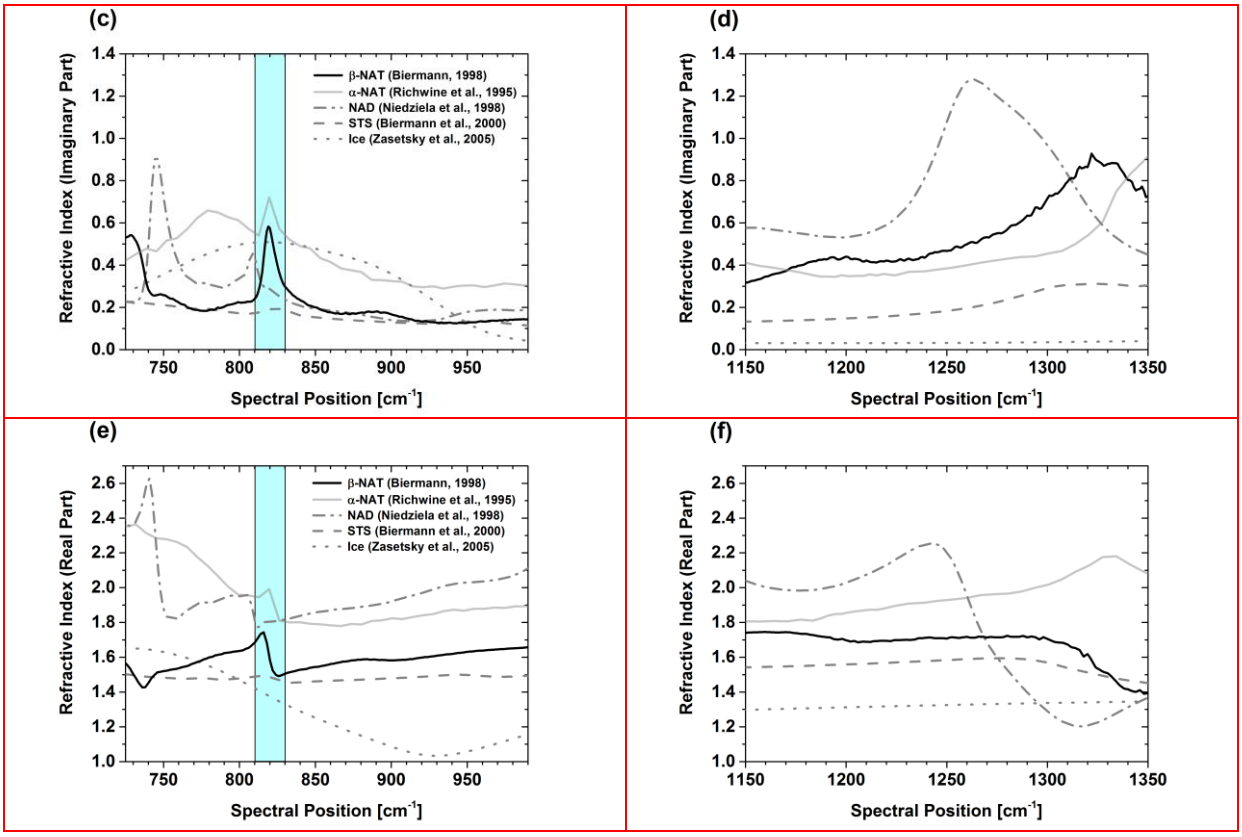

P39/L5: of β-NAT, α-NAT, NAD, STS and ice.

The authors have detected highly aspherical NAT particles, which are in accordance with lab experiments (XRD, ESEM) and Avrami calculations by Grothe et al. (2006) and Tizek et al. (2004). The main aspect ratio is 1:10 or 10:1. The authors should however indicate clearly if they assign these ratios to needles or platelets? Are optical calculations able to distinguish between these alternatives?

We would like to clarify that out of the scenarios analyzed for β-NAT (AR=0.1, 0.5, 1.0, 2 and 10), the best overall agreement is found for elongated spheroids with AR=0.1. Thereby, the choice of the extreme aspect ratios was motivated by the work of Grothe et al. (2006) (see P3/L4). However, more extreme AR values for both elongated and oblate spheroids may further improve the agreement. The modeled spectral signatures show different sensitivities to changes in AR for elongated and oblate particles due to the different contributions from absorption and scattering. However, from the scenarios analyzed we cannot tell which particle geometry would ultimately lead to the best agreement, if the AR values would be modified sufficiently. Further aspects modifying the signal are the exact particle shape (e.g. presence of edges and flat surfaces) and potential shape-dependent orientation effects. So in summary, within the scenarios analyzed best agreement is found for elongated spheroids with AR=0.1. However, we cannot exclude that other combinations of particle geometries, aspect ratios and potential shape-dependent orientation effects would favor a different particle geometry.

We modified the manuscript as follows:

P1/L28-29: Within the scenarios analyzed, the best overall agreement is found for elongated spheroids with AR=0.1.

P11/L16: The choice of the AR values is motivated by the laboratory experiments by Grothe et al. (2006), resulting in needles and platelets with similar proportions depending on the crystallization conditions.

P16/L28: Further combinations of particle shapes (e.g. including edges and flat surfaces), aspect ratios and potential shape-dependent orientation effects might further improve the agreement of simulations and observations.

Only recently Weiss et al. (2016) have shown that α-NAT has a much lower heterogeneous nucleation barrier than β-NAT, where ice acts as the heterogeneous nucleus. In a lab experiment, HNO3 was deposited from the gas phase onto an ice film and the outcome was a pure α-NAT film on top of the ice substrate – similar findings are also reported by Gao et al. (2015). This is important in view of the here presented findings, since Grothe et al (2006) found long needles with an aspect ratio of 1:10 only in the presence of ice. On the other hand platelets with a much smaller aspect ratio were found in experiments without ice. So the straightforward conclusion would be that the history of the here observed NAT particles should have involved a heterogeneous nucleation step of α-NAT on ice and a subsequent transformation of α-NAT into β-NAT. It would be interesting to note if the presence of ice can be confirmed by limb emission spectra.

See comment to referee #2: Particle backward trajectories by Molleker et al. (2014) suggest that model temperatures were too warm for ice nucleation. Furthermore, temperatures around flight altitude were clearly too warm for ice. However, ice particles might have nucleated during lee-wave-induced cooling above Greenland not resolved by the model. Therefore, ice might have been involved in the nucleation of the observed particles.

We modified the manuscript as follows:

P16/L19: The fact that best agreement is found for highly elongated particles might hint on a heterogeneous nucleation of the particles involving ice and a subsequent phase transition from α-NAT to β-NAT (Grothe et al., 2006, Iannarelli et al., 2016, Weiss et al. 2016, and references therein). While the temperatures at flight altitude were too warm for ice and α-NAT and model temperatures do not support a previous ice nucleation, Molleker et al. (2014) suggest that ice particles might have nucleated previously during lee-wave-induced cooling above Greenland not resolved by the model, enabling an ice-induced nucleation of NAT.

P20/L16: Iannarelli, R. and Rossi, M. J.: Heterogeneous Kinetics of H_2O, HNO_3 and HCl on HNO_3 hydrates (α-NAT, β-NAT, NAD) in the range 175–200 K, Atmos. Chem. Phys. Discuss., doi:10.5194/acp-2016-247, in review, 2016.

P22/L19: Weiss, F., Kubel, F., Gálvez, O., Hoelzel, M., Parker, S.F., Iannarelli, R., Rossi, M.J. and 1094 Grothe, H.: Metastable Nitric Acid Trihydrate in Ice Clouds, Angewandte Chemie I.E., 55, 1095 3276-3280, 2016; doi: 10.1002/anie.201510841, 2016.

Additionally, Tizek et al. (2004) found a stabilization of α-NAT in ice matrices. The phase transition was so much hindered by the ice that at about 200 K α-NAT could still be observed for several hours. It might be worth to check for the presence of α-NAT in the here presented spectra. Iannarelli and Rossi (2016) have estimated an enthalpy difference of 6 ± 20 kJ/mol between α- and β-NAT in favor of the latter which just about corresponds to the enthalpy difference between diamond and graphite, also in favor of the latter, with one significant difference, namely that the barrier in the carbon system is very high in contrast to the nitric acid trihydrates. However, the phase transition occurs in both systems with differing rates owing to differences in the corresponding barriers. An interesting situation arises in α-NAT because the enthalpy of evaporation of HNO3 is lower than in β-NAT by 32 ± 20

kJ/mol, but this difference is more than compensated by the increased stability of the H2O network which results in the small, but probably significant enthalpy difference in favor of β-NAT.

While the temperatures at flight altitude were too warm for the persistence of ice and α-NAT under atmospheric conditions, we now include Mie simulations for α-NAT with spherical geometry (which would be supported by the work of Grothe et al., 2006) to test for this species (see above). The results of the simulations do not support the presence of large spherical α-NAT particles.

The authors discuss a possible transformation of NAD into NAT. In Tizek et al. (2004) and Grothe et al. (2008), we have performed corresponding laboratory experiments. We may underline that we have observed α-NAD transforming into β-NAD and the respective melting of β-NAD. However, a phase change from α-NAD or β-NAD into β-NAT was of extremely low significance and should be kinetically and thermodynamically unfavorable. Also from a stoichiometric point of view, one may conclude that this would include the formation of nitric acid monohydrate or pure nitric acid, which are rather unlikely on thermodynamic grounds. Again a transformation from α-NAT into β-NAT is the most reasonable process, which also fits the observations of Weiss et al. (2016) and Gao et al. (2015).

We thank the authors of the comment for pointing out this aspect and delete the statement at P10/L26, suggesting a phase transition from NAD into NAT. As discussed above, a potential phase transition from α-NAT to β-NAT is now mentioned in the conclusions.

In this context, one might also remember the AIDA experiments performed by Stetzer et al. (2006) where no NAT but α-NAD formation had been observed. The reason might be well involved HNO3 concentrations that were larger than required for NAT formation and so led to NAD. Only recently Iannarelli and Rossi (2015) could show in laboratory experiments that increased HNO3 concentrations exposed to pure ice spontaneously led to NAD.

This very interesting aspect might help to better understand the results by Stetzer et al. (2006) and design further experiments.

References

H. Tizek, E. Knözinger, H. Grothe: "Formation and Phase Distribution of Nitric Acid Hydrates in the Mole Fraction Range $x_{HNO_3} < 0.25$: a combined XRD and IR study"; Physical Chemistry Chemical Physics, 6 (2004), p. 972 - 979.

H. Grothe, H. Tizek, D Waller, D Stokes: "The Crystallization Kinetics and Morphology of Nitric Acid Trihydrate"; Physical Chemistry Chemical Physics, 8 (2006), p. 2232 - 2239.

H. Grothe, H. Tizek, I. Ortega:"Metastable Nitric Acid Hydrates - Possible Constituents of Polar Stratospheric Clouds?"; Faraday Discussions, 137 (2008), p. 223 - 234.

F. Weiss, F. Kubel, O. Galvez, M. Hölzel, S. F. Parker, P. Baloh, R. Iannarelli, J Rossi, H. Grothe: "Metastable Nitric Acid Trihydrate in Ice Clouds"; Angewandte Chemie - International Edition, 55 (2016), 10; p. 3276 - 3280.

R. Iannarelli, M.J. Rossi: "Heterogeneous Kinetics of H_2O, HNO_3 and HCl on HNO_3 hydrates (α-NAT, β-NAT, NAD) in the range 175-200 K", submitted to Atmos. Chem. Phys. Discuss. (2016), ms. no. : acp-2016-247.

R. Iannarelli, M.J. Rossi: "The mid-IR Absorption Cross Sections of α- and β-NAT ($HNO_3 \cdot 3H_2O$) in the range 170 to 185K and of metastable NAD ($HNO_3 \cdot 2H_2O$) in the range 172 to 182K", J. Geophys. Res. Atmos. (2015), 120, doi:10.1002/2015JD023903.

O. Stetzer, O. Möhler, R. Wagner, S. Benz, H. Saathoff, H. Bunz, O. Indris: "Homogeneous nucleation rates of nitric acid dihydrate (NAD) at simulated stratospheric conditions – Part I: Experimental results", Atmos. Chem. Phys. (2006), 6, 3023–3033.

*R.-S. Gao, T. Gierczak, T. D. Thornberry, A. W. Rollins, J. B. Burkholder, H. Telg, C. Voigt, T. Peter and D. W. Fahey: "Persistent Water–Nitric Acid Condensate with Saturation Water Vapor Pressure Greater than That of Hexagonal Ice", J. Phys. Chem. A (2016), 120, 9, p. 1431–*1440